S Y N O P S I S

of the PhD Thesis

“Improving The Electrochemical Behaviors Of Sacrificial Aluminium Anode by Various Method”

Proposed to be submitted in partial fulfillment of the requirements for the award of the degree

Doctor of Philosophy

in

Metallurgy Engineering

Submitted to
Gujarat Technological University

By

Tushal Kalubhai Kyada

Enrollment No.: 219999921004

Under the Supervision of

Research Supervisor

DR. Indravadan B. Dave

Head of the Department, Metallurgy Engineering Department, Government Engineering College, Gandhinagar.

GUJARAT TECHNOLOGICAL UNIVERSITY

AHMEDABAD

February 2026

Table of Contents

1. Title of the thesis and abstract

Title of the Thesis: Improving the Electrochemical Behaviors of Sacrificial Aluminium Anode by Various Method.

Abstract:
Aluminum-based alloys are extensively used as sacrificial anodes in marine cathodic protection systems owing to their high electrochemical activity, favorable current efficiency and low density. Among these, Al-Mg alloys are particularly attractive because of their robust resistance to passivation in chloride-rich seawater. Despite their broad utilization, the combined effect of silicon additions and thermal processing on the microstructural evolution, mechanical response and electrochemical performance of Al–Mg alloys remains inadequately understood. In this work, the synergistic effects of silicon content (1.5–6 wt.%) and T6 heat treatment on the properties of Al-6.5Mg-xSi alloys were systematically investigated.

Microstructural characterization using optical microscopy as well as scanning electron microscopy and X-ray diffraction revealed that increasing silicon content significantly alters the morphology and distribution of the Mg_2Si phase. With higher silicon additions, the Mg_2Si phase evolves from coarse, flake-like particles into a finer, interconnected Chinese-script eutectic structure. These microstructural modifications contribute to a progressive increase in hardness through the formation of strengthening intermetallic phases.

Electrochemical characterization was performed in a 3.5 wt.% NaCl environment to assess the stability of the investigated alloys. Long-term corrosion rates were determined via weight loss measurements and corrosion kinetics were analyzed using potentiodynamic polarization techniques. Anode performance was assessed in accordance with the DNV-RP-B401 standard. The results indicate that silicon additions enhance depassivation behavior and shift the operating potential toward more electronegative values, which is desirable for sacrificial anode applications. However, silicon contents exceeding 1.5 wt.% were found to increase corrosion susceptibility due to intensified micro-galvanic interactions between the α-Al matrix and intermetallic phases. The application of T6 heat treatment effectively mitigates this drawback by dissolving coarse as-cast constituents and promoting the precipitation of fine, uniformly distributed Mg_2Si particles. This treatment also alters the corrosion mode from localized pitting to more uniform dissolution, a critical requirement for stable and predictable anode consumption.

The present investigation demonstrates that a balanced combination of silicon content and heat treatment is critical for achieving stable electrochemical behavior and prolonged service life in Al-Mg-Si sacrificial anodes. These insights contribute to a deeper understanding of composition-microstructure-corrosion relationships relevant to marine cathodic protection systems.

2. Brief description of the state of the art of the research topic

Aluminum and its alloys play a critical role in corrosion protection technologies, particularly in cathodic protection systems for marine, offshore, and industrial structures. Among various sacrificial anode materials, aluminum-based alloys have gained widespread acceptance due to their high electrochemical capacity, low density, cost-effectiveness, and favorable performance in chloride-rich environments such as seawater [1–3]. Compared to magnesium and zinc anodes, aluminum offers an optimal balance between driving potential, current efficiency, and consumption rate, making it suitable for long-term protection of steel structures [4,5].

The corrosion behavior of aluminum is governed by its strong tendency to form a thin, adherent oxide film (Al_2O_3) when exposed to air or aqueous environments. This passive layer provides excellent corrosion resistance under neutral conditions but limits aluminum's effectiveness as a sacrificial anode unless controlled activation is achieved [6,7]. In seawater, chloride ions can locally disrupt the oxide film, leading to pitting corrosion; however, pure aluminum often remains insufficiently active due to rapid repassivation [8,9]. As a result, alloying strategies are widely employed to suppress passivation and promote sustained anodic dissolution.

Electrochemical performance of aluminum sacrificial anodes is primarily dictated by electrode potential, current efficiency, and corrosion uniformity. Aluminum possesses a highly negative standard electrode potential (−1.66 V vs. SHE), placing it among the most active structural metals in the electromotive force (EMF) series [7]. Nevertheless, its real-world behavior is better described by the galvanic series in seawater, where oxide film formation shifts aluminum toward a more noble response compared to magnesium or activated aluminum alloys [1]. Consequently, alloyed aluminum systems such as Al–Zn, Al–Mg–In, and Al–Zn–Mg–Si have been developed to maintain activation and ensure predictable anodic performance [9,10].

Current efficiency is a key parameter in sacrificial anode applications, as it defines the fraction of electrical charge that contributes to effective metal dissolution. Aluminum alloys typically exhibit higher current efficiencies than magnesium anodes and greater electrochemical capacity than zinc-based systems, making them attractive for long-duration service [29]. The addition of minor alloying elements such as zinc, indium, tin, gallium, and silicon has been shown to disrupt the passive oxide film, enhance anodic dissolution, and improve efficiency by stabilizing the electrochemical potential [11–14].

Among alloying elements, magnesium plays a significant role by strengthening aluminum through solid-solution hardening while also contributing to electrochemical activation [15]. In Al-Mg-Si alloys, silicon further modifies the microstructure by forming Mg_2Si precipitates, which influence grain refinement, mechanical hardness, and corrosion behavior [14,16].

However, excessive silicon content can increase susceptibility to intergranular corrosion due to the formation of electrochemically active Mg_2Si particles along grain boundaries, leading to micro-galvanic coupling with the aluminum matrix [14,16]. This highlights the importance of compositional control in achieving a balance between activation and corrosion uniformity.

Passivation remains one of the major challenges limiting the effectiveness of aluminum sacrificial anodes. Thermodynamically, aluminum oxide is highly stable, with a Pilling–Bedworth ratio of approximately 1.28, indicating the formation of a dense and protective oxide film [9]. While beneficial for structural applications, this oxide layer reduces anodic activity in cathodic protection systems. Environmental factors such as pH, temperature, and chloride concentration strongly influence oxide stability and breakdown [17]. In highly alkaline or acidic conditions, the oxide layer may dissolve, whereas under moderate conditions, it can become increasingly resistant, leading to reduced anode efficiency.

To overcome passivation, depassivation strategies are widely employed. Alloying remains the most effective approach, as specific elements weaken the oxide film and promote continuous dissolution [11,18]. Studies have shown that zinc additions up to approximately 6 wt.% significantly increase anode efficiency by facilitating passive film breakdown through β-phase formation [11]. Similarly, tin and gallium additions create localized activation sites that improve corrosion uniformity and current output [19,20]. Silicon, when carefully controlled, contributes to grain refinement and more uniform dissolution, though excessive amounts may be detrimental [14]. In addition to alloying, heat treatment plays a crucial role in tailoring the microstructure and performance of aluminum alloys. Solution heat treatment followed by quenching enables the uniform dissolution of alloying elements, while aging treatments promote the controlled precipitation of strengthening phases such as Mg_2Si in Al–Mg–Si systems [21–23]. Artificial aging (T6 condition) is particularly effective in enhancing hardness and mechanical stability by refining precipitate distribution, whereas overaging (T7 condition) improves stress corrosion resistance at the expense of peak strength [24–26]. Heat treatment also influences corrosion behavior by modifying precipitate morphology and reducing localized galvanic interactions, thereby promoting more uniform anodic dissolution [26].

Recent research emphasizes the need to understand the combined effects of alloy chemistry and thermal processing on electrochemical performance. While extensive studies exist on individual alloying elements and conventional aluminum systems, comparatively limited work has focused on the synergistic role of silicon content and heat treatment in Al-Mg-Si sacrificial anodes. Addressing this gap is essential for optimizing anode efficiency, corrosion uniformity, and service life in demanding marine environments.

3. Definition of the problem

The present research on aluminum-based sacrificial anodes addresses several critical gaps in the existing understanding of their behavior and performance:

Conventional aluminum anodes often suffer from non-uniform dissolution, localized pitting and unstable operating potentials during service, leading to reduced utilization efficiency and shortened service life. These limitations restrict their reliability in aggressive chloride-rich marine environments.

Various approaches, including alloying and heat treatment, have been explored to improve anode performance. Alloying with magnesium and silicon is known to influence microstructural features, activation behavior and corrosion response. Nevertheless, most existing studies focus on individual alloying effects or as cast conditions, while the combined influence of alloy composition and thermal processing remains insufficiently investigated. In particular, the role of heat treatment in modifying phase morphology, precipitate distribution, and micro-galvanic interactions in aluminum sacrificial anodes is not yet fully understood.

This research aims to systematically examine the synergic effects of magnesium and silicon additions along with controlled heat treatment on the microstructure, hardness and electrochemical behavior of Al–Mg–Si alloys, with the goal of developing high-efficiency sacrificial anodes exhibiting stable potential, uniform dissolution and improved service performance.

4. Objectives and scope of the work

The present research is designed to address the identified research gaps and key challenges associated with aluminum-based sacrificial anodes. The electrochemical behavior of aluminum sacrificial anodes can be studied by adding magnesium and silicon with the following potential objectives.

1. To fabricate aluminum-based sacrificial anodes alloyed with magnesium and silicon, with particular emphasis on the formation and distribution of the Mg_2Si phase for enhanced anodic performance.
2. To examine the influence of heat treatment on the evolution and morphology of the Mg_2Si phase, and its role in modifying microstructural characteristics.
3. To evaluate the synergistic effects of alloying and heat treatment on the microstructure, mechanical hardness, and electrochemical behavior of the developed Al-Mg-Si alloys.

Scope of Work: The primary aim of this research is to enhance the performance of Al–6.5% Mg sacrificial anodes through two complementary approaches: alloying with silicon (Si) and the application of controlled heat treatment.

In the first approach, silicon is added to the Al–6.5% Mg alloy in varying concentrations (1.5%, 3%, 4.5%, and 6% by weight) to evaluate its incorporation and influence on alloy performance. The hardness of the developed alloys is compared with that of pure aluminum to assess the individual and combined effects of magnesium and silicon on mechanical properties. Microstructural characterization is carried out using optical microscopy and scanning electron microscopy (SEM) to examine the influence of silicon addition on phase morphology and distribution. Phase identification is performed using X-ray diffraction (XRD). The corrosion behavior of the base Al–6.5% Mg alloy and the Si-modified alloys is evaluated using the weight loss method and potentiodynamic polarization testing. Anode performance of the as cast alloys is assessed in accordance with the DNV-RP-B401 standard.

The second approach focuses on the heat treatment of the developed alloys. Hardness measurements of heat-treated samples are compared with those of the as-cast condition to quantify the effect of thermal processing. Microstructural changes induced by heat treatment are examined using optical microscopy and SEM and their influence on corrosion behavior is evaluated through weight loss and potentiodynamic testing. Anode performance of the heat-treated samples is also evaluated following the DNV-RP-B401 guideline.

The synergistic effects of alloying and heat treatment are investigated through an integrated assessment of microstructure, phase morphology, corrosion behavior and anode performance to determine their role in improving the electrochemical behaviors of Al–6.5% Mg sacrificial anodes.

5. Original contribution by the thesis

This thesis presents a systematic investigation aimed at improving the performance of aluminum-based sacrificial anodes for marine cathodic protection applications. The primary contribution lies in evaluating the combined effects of silicon alloying and heat treatment on the microstructural evolution, phase morphology, mechanical hardness, corrosion behavior and anodic performance of Al–6.5% Mg alloys. The study demonstrates that controlled silicon additions in the range of 1.5–6 wt.% significantly influence the formation and distribution of the Mg_2Si phase, thereby affecting anodic dissolution behavior. In contrast to earlier studies focused mainly on as cast alloys or isolated alloying effects, this work highlights the critical role of heat treatment in refining microstructure, modifying phase characteristics and reducing micro-galvanic interactions, leading to more uniform corrosion behavior. Clear relationships between microstructure and electrochemical performance are established through microstructural characterization, hardness evaluation and electrochemical testing. Anode performance is systematically assessed for both as cast and heat treated conditions in accordance with the DNV-RP-B401 standard. The results confirm that appropriate selection of silicon content and heat treatment parameters enables stable operating potential, uniform dissolution, and improved utilization efficiency, thereby extending the service life of Al-Mg-Si sacrificial anodes in marine environments.

6. The methodology of research, results

This section describes the materials, experimental procedures and characterization techniques employed in the study. It includes details of raw materials, alloy preparation, casting and heat treatment processes, experimental setup, and testing methods. The flow of experimental work is shown in figure 6.1. It involved the fabrication of Al-Mg-Si alloys and heat treatment followed by chemical analysis, mechanical property evaluation, microstructural and phase characterization, corrosion testing, post-corrosion analysis and anode efficiency measurement.

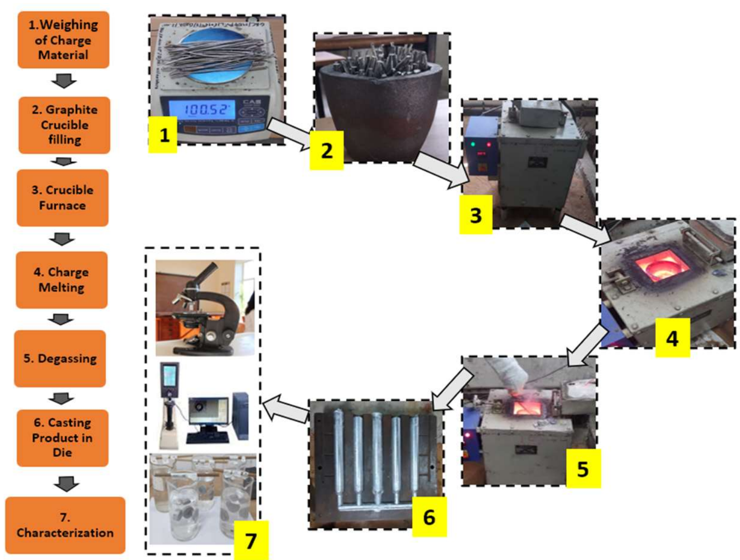

Figure 6-1 Flow chart of experimental work

6.1 Experimental Work and Methodology

6.1.1 Raw Materials

Commercially pure aluminum (99.7 wt.%), silicon (99.9 wt.%), and magnesium (98.8 wt.%) were used for alloy preparation. Aluminum wire, containing minor impurities, was obtained from a GETCO contractor, while high-purity magnesium and silicon were sourced from C.K. Enterprise, Vadodara, and Riddant Aluminium Pvt. Ltd., Surat, respectively. The chemical compositions of the raw materials are listed in Table 1.

Table 1. Chemical composition of commercially pure aluminium wire

	Al %	Si %	Mg %	Fe %	Cu %	Mn %	Zn %	Ti %	Pb %	O %
Aluminium wire	99.7	0.25	-	0.4	0.10	0.07	0.04	0.01	0.05	-
Silicon	0.005	99.9	-	0.01	-	-	-	0.001	-	0.02
Magnesium	-	-	98.8	-	-	-	-	-	-	1.24

6.1.2 Fabrication of Al-Mg-Si Alloys

Al-Mg-Si alloys were prepared using an electric resistance furnace at the departmental facilities of Dr. S. & S. S. Ghandhy College of Engineering & Technology, Surat. As shown in figure 6-2. Commercially pure aluminum was melted in a graphite crucible at approximately 800 °C, followed by the controlled addition of magnesium (6.5 wt.%) and silicon (0–6 wt.%). The molten alloy was continuously stirred to ensure uniform distribution of alloying elements. Casting was carried out using a preheated grey cast iron metallic die to produce rod-shaped specimens. Proper cleaning and drying of crucibles and dies were maintained throughout the process to minimize contamination and ensure casting quality.

Figure 6-2 Electric Resistance Furnace at Dr. S & S. S. Ghandhy College of Engineering & Technology, Surat.

The furnace charge was calculated to achieve the desired Al–Mg–Si alloy compositions. Five alloys were designed with a constant magnesium content of 6.5 wt.% while varying silicon content from 0 to 6 wt.% in steps of 1.5 wt.%. The required quantities of magnesium and silicon were calculated based on the total charge weight using standard percentage relations. Pure aluminum constituted the balance of the charge.

6.1.3 Heat Treatment of developed Al-Mg-Si Alloys

The developed Al–Mg–Si alloys were subjected to heat treatment using a muffle furnace at the departmental facilities of Dr. S & S. S. Ghandhy College of Engineering & Technology, Surat as shown in figure 6-3. The heat treatment cycle consisted of solution treatment at 540 °C for 1 hour to dissolve alloying elements, followed by immediate water quenching to retain a supersaturated solid solution. Subsequently, artificial aging was carried out at 200 °C for 4 hours to promote precipitation hardening, and the samples were finally air cooled to stabilize the microstructure.

Figure 6-3 Muffle furnace at Dr. S & S. S. Ghandhy College of Engineering & Technology, Surat

The detailed testing of the developed alloys in both as cast and heat treated conditions is illustrated in Figure 6.4. Initially, chemical composition analysis was carried out using optical emission spectrometer, to confirm the alloy chemistry. Subsequently, the alloys were evaluated for mechanical properties, with particular emphasis on hardness testing. Microstructural characterization was performed through standard metallographic preparation followed by optical microscopy to examine phase distribution and structural features.

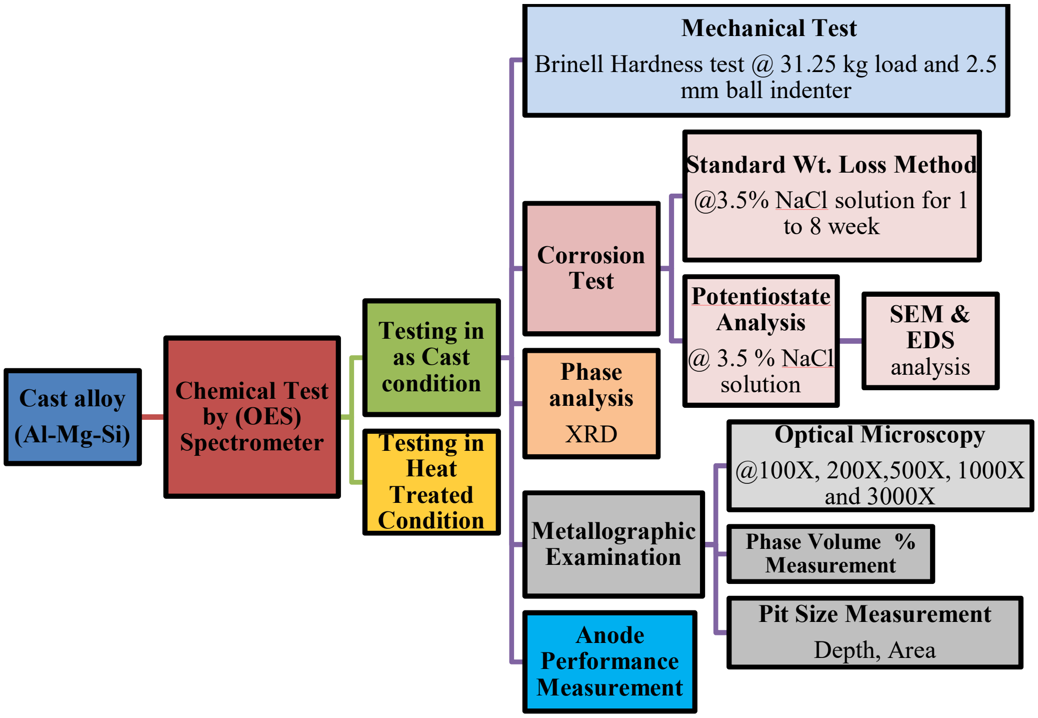

Figure 6-4 Detailed testing Plane for the experimental study

Corrosion behavior was assessed by immersing the samples in a 3.5% NaCl solution. The corrosion performance was evaluated using weight loss measurements and potentiodynamic polarization techniques. After corrosion testing, the sample surfaces were examined by visual inspection and Scanning Electron Microscopy (SEM) to study surface degradation, corrosion morphology, and associated microstructural changes. Additionally, the sacrificial anode performance of the developed alloys was evaluated as per the DNV RP B401 standard**.**

A. **Chemical Analysis**

The chemical composition of the developed alloy was determined using a Bruker Q4 TASMANIA CCD-based optical emission spectrometer at Aadhya Metal Testing, Baroda, following ASTM E1251:2017. Cleaned cast samples were spark-excited, and emitted spectra were analyzed to quantify elemental composition accurately.

B. **Hardness Evaluation**

Hardness of the developed Al–Mg–Si alloys was measured using the Brinell hardness test as per ASTM E10. Samples were sectioned, cleaned, and polished using 1200-grit paper to obtain a smooth surface. Testing was performed using a 2.5 mm ball indenter under a load of 31.25 kg applied for 10 s. The indentation diameter was measured optically and used to calculate the Brinell hardness number.

C. **Microstructural and Phase Analysis**

Metallographic samples were prepared through standard procedures to obtain a representative and defect-free surface for microstructural examination. Specimens were sectioned from cast rods into dimensions of approximately 20 mm diameter and 15 mm height using an automatic cutting machine. Grinding was carried out using emery belts followed by wet grinding with silicon carbide papers ranging from 500 to 2000 grit. Final polishing was performed on rotating cloth wheels using an Al_2O_3 suspension in distilled water to achieve a mirror-like surface.

The polished samples were etched using Keller's reagent for about 10 s to reveal microstructural features. After rinsing and drying, microstructural and phase analyses were conducted using an Olympus DSX1000 digital optical microscope and a JEOL JSM 7900F SEM equipped with EDS for detailed morphological and compositional evaluation.

X-ray diffraction (XRD) analysis was performed to identify the crystalline phases present in the alloy using a Panalytical X'Pert Pro diffractometer at Maharaja Sayajirao University, Baroda. Cu Kα radiation (λ = 1.5406 Å) was employed for phase identification. Cylindrical specimens (20 mm diameter, 2 mm thickness) were ground using 500–2000 grit SiC papers and polished with alumina suspension prior to analysis. The obtained diffraction patterns were analyzed using dedicated software and matched with standard reference data to confirm the phases present and assess the crystallographic structure of the alloy.

D. Corrosion Behavior Study

The corrosion behavior of the developed Al-Mg-Si alloys was evaluated using two complementary techniques: the standard weight loss method and potentiodynamic polarization. These methods provide both long-term corrosion rate data and electrochemical characteristics of the alloys. Weight loss testing was conducted in accordance with ASTM G1-03 (2017) using a 3.5 wt.% NaCl solution to simulate a chloride-rich marine environment. Cylindrical specimens (20 mm diameter, 10 mm height) were ground to a smooth finish, cleaned, weighed, and immersed for a total duration of eight weeks. At weekly intervals, specimens were removed, cleaned, dried, and reweighed. The corrosion rate was calculated based on weight loss, exposed surface area, density, and exposure time. The average corrosion rate was obtained from three specimens to improve accuracy.

Potentiodynamic polarization studies were carried out following ASTM G5 using a Gamry Reference 600 potentiostat. A three-electrode cell configuration was employed with the alloy as the working electrode, graphite as the counter electrode, and a saturated calomel electrode as the reference. Polarization curves were generated to determine corrosion potential (Ecorr) and corrosion current density (Icorr). Post-corrosion evaluation included visual inspection and SEM analysis to examine surface degradation, pit formation, oxide films, and corrosion products, providing insight into corrosion mechanisms.

E. Assessment of Anode Performance

The sacrificial anode performance of the developed alloys was evaluated in accordance with DNV RP B401 guidelines to determine efficiency, consumption rate and electrochemical behavior. The test was conducted using a mild steel vessel containing 11 L of natural seawater as the electrolyte. A standard copper coulometer solution was prepared as per ASTM G97 to measure charge transfer during testing. Experimental Set up for anode performance measurement is shown in figure 6-5.

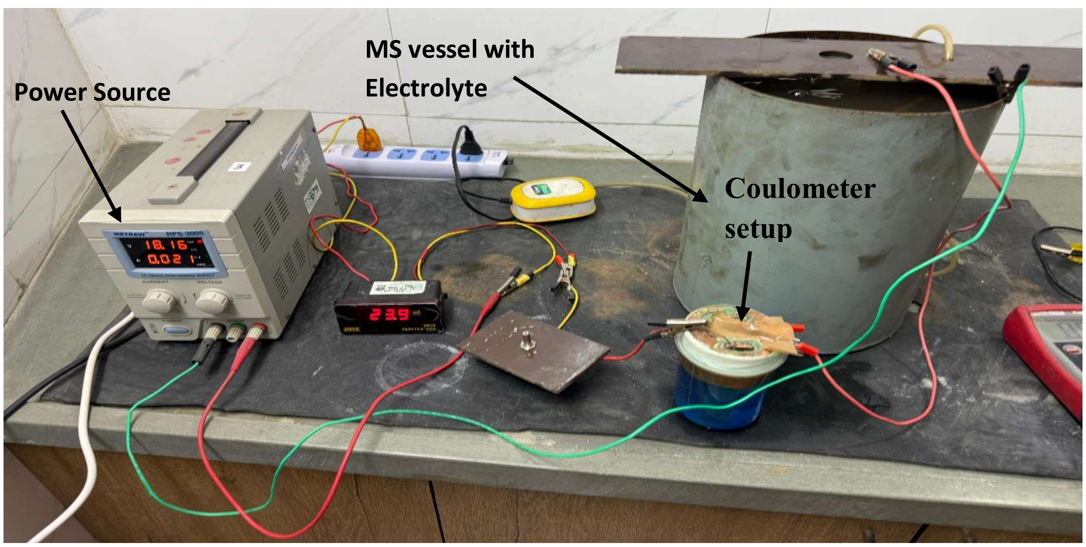

Figure 6-5 Experimental Set up for anode performance measurement as per DNV RP B401

Prior to testing, anode specimens were cleaned with methanol, while post-test cleaning was carried out using a chromium trioxide–phosphoric acid solution to remove corrosion products. The cylindrical anode specimen was mounted in the test setup with an ammeter and variable resistance connected in series to regulate current. Current densities of 1.5, 0.4, 4, and 15 mA/cm² were applied sequentially, each maintained for 24 ± 1 h over four consecutive days with continuous air purging of the electrolyte.

Open-circuit and closed-circuit potentials were recorded, and current output was monitored periodically. After completion of the test, the specimens were cleaned, dried, and weighed to determine material loss. Key performance parameters such as consumption rate (kg/A·yr), current capacity (Ah/kg), and potential behavior were evaluated to assess anodic efficiency, durability, and compliance with DNV RP B401 standards.

6.2 Results and Discussion

6.2.1 Effect of Silicon Addition on the Composition of Aluminum Alloys

Optical emission spectroscopy (OES) results (Table 2) confirm successful silicon incorporation in Al–6.5%Mg alloys. Measured Si contents were 1.61, 3.03, 4.41, and 5.61 wt.% for alloys A–D, closely matching the targeted additions of 1.5, 3.0, 4.5, and 6.0 wt.%. Magnesium content remained nearly constant (6.63–6.76 wt.%) across all compositions, indicating minimal loss during alloying.

Table 2 Chemical composition of Al–6.5%Mg alloys with varying Si additions (wt.%) determined by OES.

Alloy / Elements	Mg %	Si %	Fe %	Cu %	Mn %	Zn %	Ti %	Pb %	Al %
Base Alloy (Al-6.5%Mg)	6.47	0.25	0.47	0.11	0.06	0.04	0.01	0.06	92.48
A (Al-6.5%Mg1.5%Si)	6.71	1.61	0.47	0.10	0.06	0.03	0.012	0.05	90.89
B (Al-6.5%Mg-3%Si)	6.76	3.03	0.47	0.09	0.05	0.04	0.011	0.04	89.43
C (Al-6.5%Mg-4.5%Si)	6.63	4.41	0.50	0.11	0.06	0.09	0.016	0.06	88.02
D (Al-6.5%Mg-6%Si)	6.76	5.61	0.54	0.11	0.06	0.03	0.014	0.06	86.70

With increasing silicon content, aluminum concentration decreased from 92.48 wt.% (base alloy) to 86.70 wt.% (6% Si alloy), reflecting substitutional alloying. Trace elements such as Fe (0.47-0.54 wt.%), Cu (0.09-0.11 wt.%), Mn (~0.06 wt.%), Zn (0.03-0.09 wt.%), Ti (0.011-0.016 wt.%), and Pb (~0.05 wt.%) showed minor variations and remained within acceptable limits. The achieved silicon levels are adequate to promote Mg_2Si intermetallic formation, influencing subsequent microstructural and property evolution.

6.2.2 Effect of Silicon Addition on the Microstructure of Al-Mg-Si Alloys

A. As Cast Microstructural Characteristics of Al–6.5Mg–xSi Alloys

Figure 6-6 (a-e) show the optical microstructures of as-cast Al-6.5Mg and Al-6.5Mg-xSi alloys (x=1.5-6 wt.% Si) at 1000X magnification. The base alloy consists of a dual-phase structure comprising α-Al (bright matrix) and β-Al_3Mg_2 (dark intermetallic), consistent with the Al-Mg phase diagram. With silicon addition, the dominant secondary phase shifts to Mg_2Si, formed by the reaction between Mg and Si.

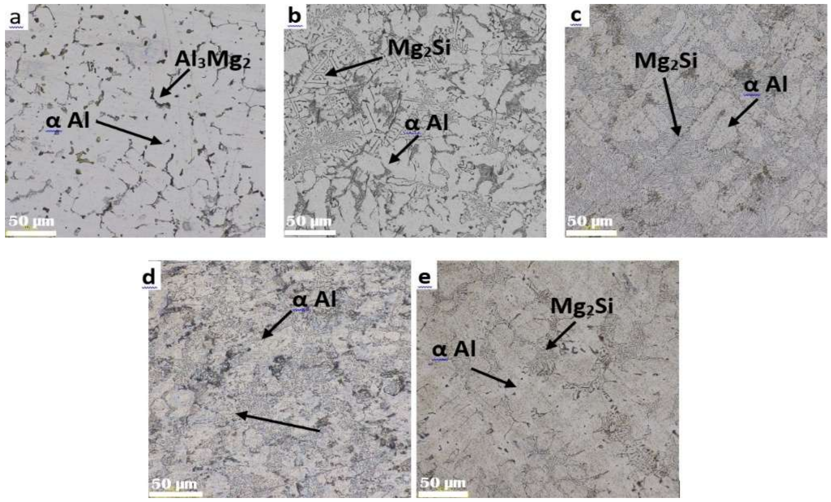

Figure *6-6* Microstructure of Al–6.5 %Mg alloys with varying Si content: (a) Al–6.5 %Mg, (b) Al–6.5 %Mg–1.5 %Si, (c) Al–6.5 %Mg–3 %Si, (d) Al–6.5 %Mg–4.5 %Si, and (e) Al–6.5 %Mg–6 %Si at 1000 X magnification, showing the evolution of Mg_2Si phases with increasing Si.

At 1.5 wt.% Si, Mg_2Si appears as fine, flake-like particles uniformly distributed in the α-Al matrix. Increasing Si content to 3 and 4.5 wt.% results in coarser, lamellar and rod-like Mg_2Si morphologies, while at 6 wt.% Si a fine, interconnected "Chinese script" eutectic network forms along grain boundaries [27,28]. SEM/EDS and XRD analyses confirm the presence of α-Al and Mg_2Si phases as shown in figure 6-7 and figure 6-8. Increasing Si content reduces the α-Al volume fraction and increases Mg_2Si density, leading to enhanced hardness but increased susceptibility to localized corrosion at higher Si levels due to micro-galvanic effects.

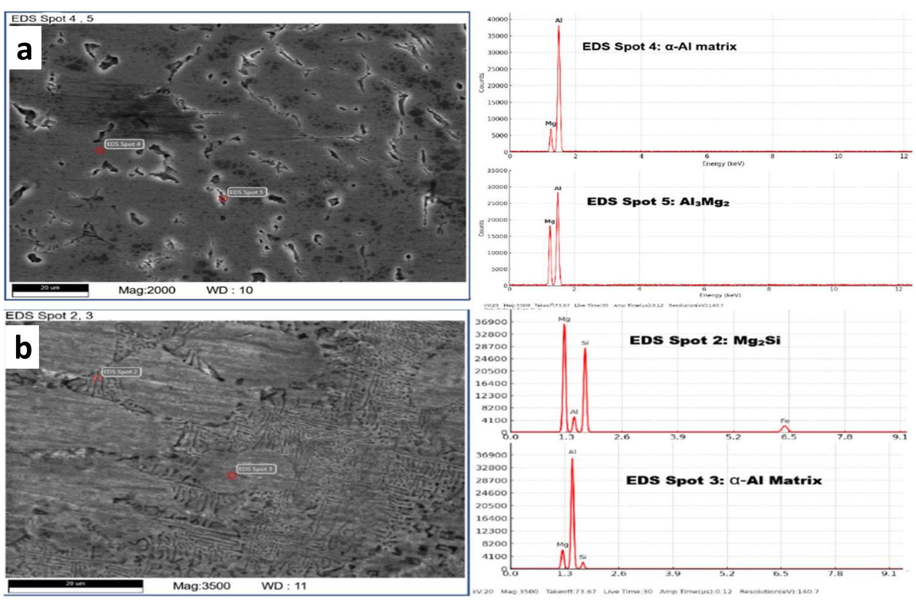

Figure 6-7 SEM micrograph with marked analysis location (Spots) and corresponding EDS spectrum, confirming the presence of the phase α-Al matrix, Al_3Mg_2 and Mg_2Si.

(a) Al-6.5Mg (b) Al-6.5Mg-3%Si alloys

XRD confirms α-Al, Al_3Mg_2 and Mg_2Si phases across all Si levels. Fine Mg_2Si at 1.5 wt.% Si improves hardness and corrosion resistance, while higher Si (3-6 wt.%) produces coarser, interconnected Mg_2Si that maximizes hardness but increases embrittlement and corrosion susceptibility.

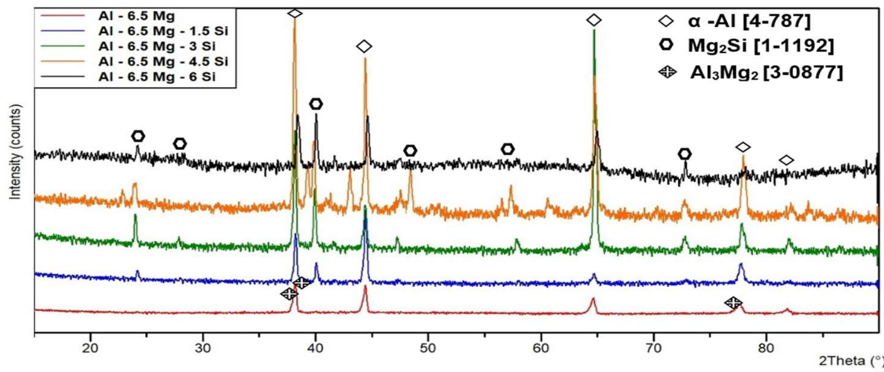

Figure 6-8 X-ray diffraction (XRD) patterns of the developed Al–Mg–Si alloys, showing the presence of α-Al, Mg_2Si, and Al_3Mg_2 phases.

B. Effect of T6 Heat Treatment on Microstructure and Phase Evolution

Following T6 heat treatment, the microstructure of Al–6.5Mg–xSi alloys consists of an α-Al matrix with finely dispersed Mg_2Si precipitates, in accordance with the Al-Mg-Si ternary phase diagram. During solution treatment, coarse Mg_2Si phases dissolve into the matrix, forming a supersaturated solid solution. Subsequent artificial aging results in the reprecipitation of Mg_2Si as fine, uniformly distributed particles, regardless of the initial as-cast morphology.

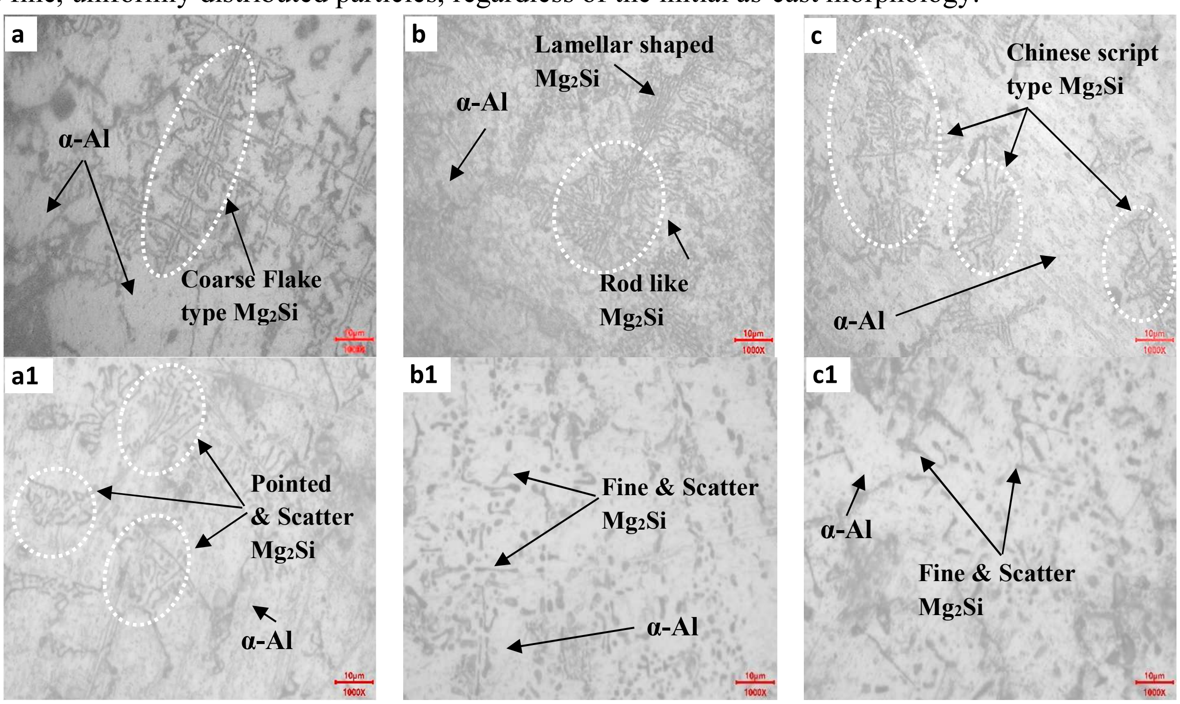

Figure 6-9 Microstructures of Al–6.5Mg–xSi alloys in as-cast (a–c) and heat treated (a1–c1) conditions for 1.5%, 3%, and 6% Si at 1000× magnification.

The application of T6 heat treatment (solution treatment followed by artificial aging) significantly alters the distribution and morphology of Mg_2Si precipitates as illustrated in figures 6-9 (a1–c1). During solution treatment, the coarse Mg_2Si phases dissolve into the α-Al matrix forming a supersaturated solid solution. This process eliminates the heterogeneous primary phases originally observed in flake-like, rod-shaped, and Chinese script morphologies. [29–32]. Upon subsequent artificial aging, the Mg_2Si phase reprecipitates in a radically altered state, where the original coarse and continuous networks are replaced by fine, dispersed, and "point-like" intermittent formations regardless of the initial as-cast structure, all three alloy variants exhibit a convergence toward this fine, scattered Mg2Si distribution, which is instrumental in enhancing the mechanical and electrochemical properties of the material [33].

6.2.3 Effect of Silicon Addition on the Hardness of Aluminum Alloys

Brinell hardness testing was carried out using a 2.5 mm diameter steel ball indenter under a load of 31.25 kg, following ASTM E10 standards. Measurements were taken at five different positions on each sample and the average values with standard deviations are presented in Table 3 and Figure 6-10.

Table 3 Brinell hardness values of pure Al, Al–6.5%Mg, and Al–6.5%Mg–Si alloys in as-cast and heat-treated conditions.

Alloy Composition	As-Cast Avg.	Std. Dev.	Heat-Treated Avg.	Std. Dev.
Pure Al	38	1.1	–	–
Base Alloy (Al–6.5%Mg)	56	2.3	–	–
A (Al–6.5%Mg–1.5%Si)	82	1.9	75	1.2
B (Al–6.5%Mg–3%Si)	67	1.7	82	1.6
C (Al–6.5%Mg–4.5%Si)	70	2.2	103	2.0
D (Al–6.5%Mg–6%Si)	83	2.9	107	2.2

The as-cast hardness of pure aluminum was 38 HB, consistent with its soft, ductile nature. The incorporation of 6.5 wt.% Mg substantially increased hardness to 56 HB, demonstrating the solid-solution strengthening effect of Mg in the Al matrix [27]. Hardness is greatly improved due to the formation of the Al_3Mg_2 (beta) phase [34].

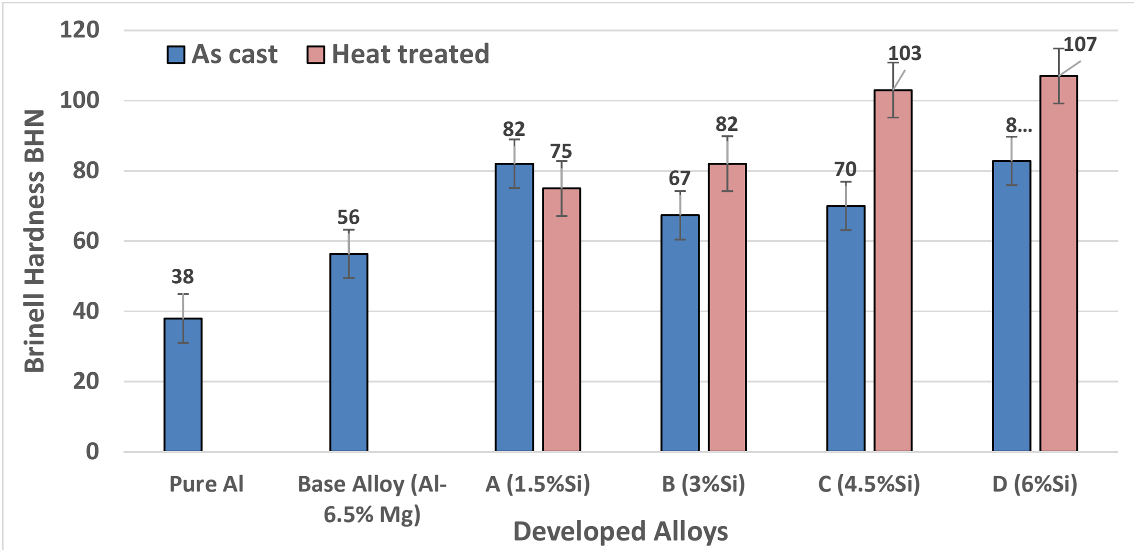

Figure 6.10 Effect of Si addition and heat treatment on hardness of Al-6.5% Mg alloys

Silicon addition significantly influenced hardness. The 1.5 wt.% Si alloy exhibited a sharp increase to 82 HB due to refined α-Al dendrites and uniform Mg_2Si and Al_3Mg_2 dispersion, which effectively hinder dislocation motion [35–37]. Intermediate Si levels (3–4.5 wt.%) showed reduced hardness (67–70 HB) owing to Mg_2Si coarsening. At 6 wt.% Si, hardness increased again to 83 HB due to a higher intermetallic phase density.

Heat treatment further enhanced hardness, particularly at higher Si contents. While the 1.5 wt.% Si alloy showed a slight decrease (82 to 75 HB), alloys with 3, 4.5, and 6 wt.% Si increased to 82, 103, and 107 HB, respectively, due to precipitation hardening by fine Mg_2Si. Overall, optimized Si addition combined with heat treatment significantly improves hardness through solid-solution and precipitation strengthening.

6.2.4 Corrosion Analysis

A. **Corrosion study by Weight Method**

Figure 6-11 shows corrosion rate variation over 8 weeks for as-cast Al–6.5Mg–xSi alloys measured by the weight-loss method. The base Al–6.5Mg alloy exhibited stable and relatively low corrosion rates, peaking at ~0.31 mpy and decreasing to 0.24 mpy at 8 weeks. Addition of 1.5 wt.% Si slightly reduced the peak corrosion rate to ~0.28 mpy, indicating improved corrosion stability. In contrast, higher Si contents (3-6 wt.%) resulted in progressively increased corrosion rates, with the 6 wt.% Si alloy reaching the highest value (~0.37 mpy). This behavior is attributed to the transition from finely dispersed Mg_2Si particles at low Si levels to coarse, semi-continuous Mg_2Si networks at higher Si contents, which enhance micro-galvanic coupling and promote localized corrosion [38,39].

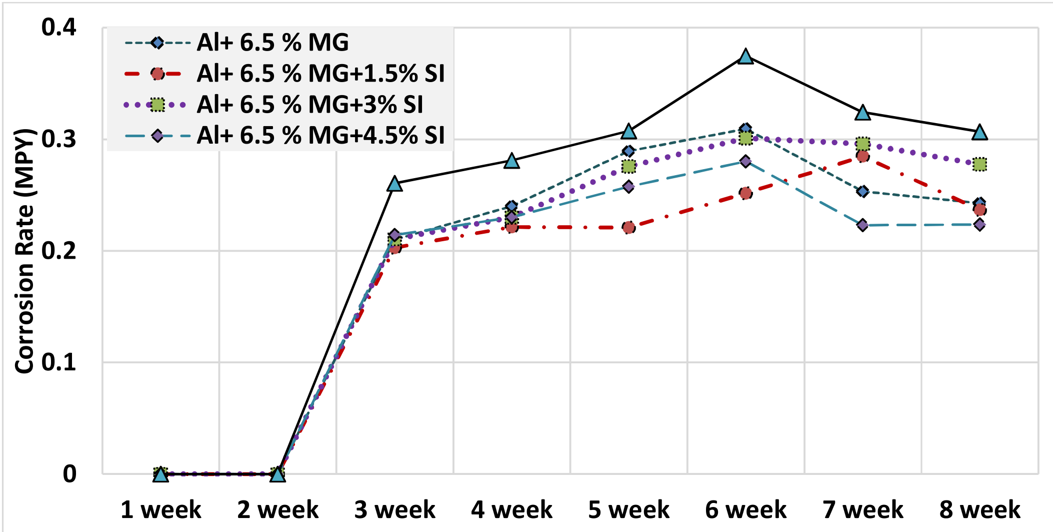

Figure 6-11 Variation of corrosion rates over time for Al–6.5 %Mg alloys with different Si contents measured using the standard weight loss method in 3.5 % NaCl solution.

After heat treatment, corrosion behavior improved for low-Si alloys due to the redistribution and refinement of Mg_2Si precipitates, leading to more uniform corrosion. Alloys with higher Si content, although benefiting from refined precipitates, still exhibited relatively higher corrosion rates owing to increased Mg_2Si volume fraction [40–42]. Surface examination after exposure revealed pit initiation within two weeks, with pit size and severity increasing with both Si content and exposure duration. Figure 6-12 show pit size measurement after 6 week of exposure to corrosive environment.

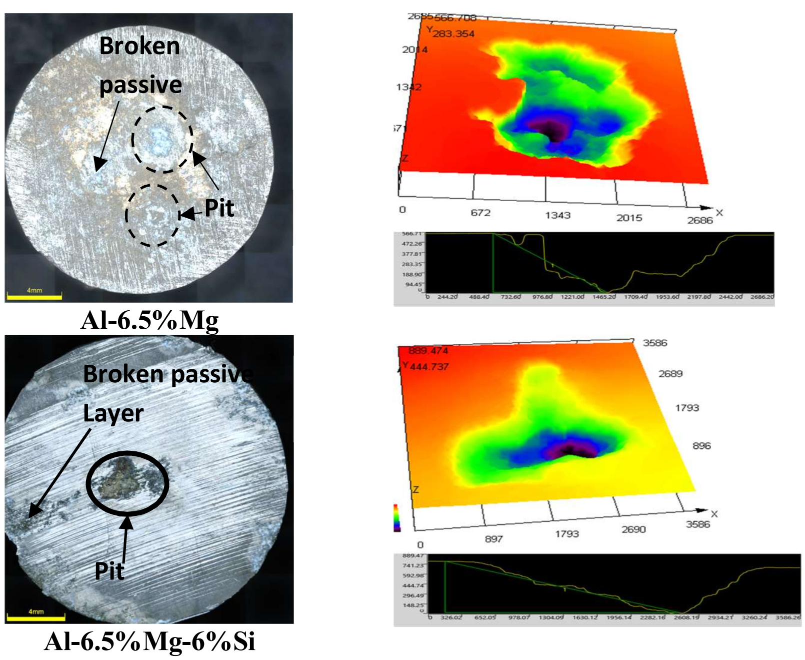

Figure 6-12 Surface morphology and pit dimension measurements of Al–6.5 %Mg–xSi alloys after 6 weeks of exposure to 3.5 % NaCl solution.

B. Potentiodynamic polarization Analysis

Table 5 presents the electrochemical data obtained from potentiodynamic polarization tests. In the as cast state, Ecorr shifts to less negative values with increasing Si (−852 mV for Al–6.5Mg to −599 mV for 3% Si), indicating reduced driving potential. The 1.5 wt.% Si alloy shows the lowest Icorr (0.41 µA/cm²), reflecting improved surface stability due to fine Mg_2Si dispersion. Higher Si contents (3–6 wt.%) exhibit increased Icorr (up to 3.62 µA/cm²), attributed to coarse and continuous Mg_2Si networks that promote micro-galvanic coupling and localized corrosion.

Table 5. Ecorr and Icorr values of Al–6.5%Mg–xSi alloys in 3.5 wt.% NaCl under as cast and heat treated condition

Name	Condition	Ecorr (mV)	Icorr (µA/cm^2)
Al+6.5%Mg	As Cast	-852.0 ±6.5	1.520 ±0.03
Al+6.5%Mg+1.5%Si		-610 ±4.3	0.41±0.01
Al+6.5%Mg+3% Si		-599.0 ±5.0	1.690 ±0.03
Al+6.5%Mg+4.5% Si		-610 ±4.8	2.584 ±0.05
Al+6.5%Mg+6%Si		-677.0 ±6.0	3.620 ±0.07
Al+6.5%Mg+1.5%Si	Heat Treated	–955±7.5	7.51±0.10
Al+6.5%Mg+3% Si		–858±6.0	2.18±0.05
Al+6.5%Mg+4.5% Si		-1.03±8.0	1.30±0.03
Al+6.5%Mg+6%Si		–946±6.0	4.64±0.08

After T6 heat treatment, all alloys display more negative Ecorr values (−858 to −955 mV), indicating increased anodic activity. However, Icorr remains lowest for the 4.5 wt.% Si alloy (1.30 µA/cm²), suggesting enhanced corrosion uniformity due to refined, discontinuous Mg_2Si precipitates. In contrast, the 1.5 wt.% and 6 wt.% Si alloys show significantly higher Icorr values (7.51 and 4.64 µA/cm², respectively), likely due to solute-depleted zones and residual galvanic effects, which reduce film stability despite higher driving potential [43–46]. The dissolution of these coarse phases and their subsequent reprecipitation as fine, intermittent "point-like" formations radically alters the electrochemical surface area. The scattered distribution of Mg2Si educes the continuity of the cathodic sites, which generally enhances the uniformity of the anodic dissolution [47].

6.2.5 Anode Performance Measurement

The sacrificial anode performance of Al–6.5Mg–xSi alloys was evaluated as per DNV RP-B401, using anode capacity and consumption rate (Table 6). The results confirm a non-linear dependence of performance on Si content. In the as-cast condition, increasing Si from 1.5 to 3 wt.% reduces anode capacity from 2136.7 to 1749.9 A·h/kg, with the 3 wt.% Si alloy showing the highest consumption rate (5.0 kg/A·year) due to non-uniform dissolution. In contrast, the 6 wt.% Si alloy exhibits superior performance, achieving a maximum anode capacity of 2781.5 A·h/kg and the lowest consumption rate of 3.15 kg/A·year, exceeding typical Al–Mg anode capacities.

Table 6 Experimental data and electrochemical performance parameters for as cast and heat treated Al-6.5Mg-Si sacrificial anodes.

Sr.No	Alloy Name	Anode capacity (Amp.hr/kg)	Consumption Rate kg/Amp*year
		As Cast	
1	**Al-6.5Mg**	2701.484323	3.2427
2	**Al-6.5Mg-1.5Si**	2136.720345	4.0997
3	**Al-6.5Mg-3Si**	1749.923552	5.0059
4	**Al-6.5Mg-4.5Si**	1623.977274	5.3942
5	**Al-6.5Mg-6Si**	2781.485862	3.1494
		Heat Treated	
1	**Al-6.5Mg-1.5Si**	2135.843698	4.1014
2	**Al-6.5Mg-3Si**	1769.381938	4.9509
3	**Al-6.5Mg-4.5Si**	1677.392706	5.2224
4	**Al-6.5Mg-6Si**	1680.185196	5.2137

A. Effect of Heat Treatment

T6 heat treatment has a composition-dependent effect [41,48]. Low-Si alloys show marginal changes, while the 6 wt.% Si alloy suffers ~65% performance loss, with consumption rate increasing from 3.15 to 5.21 kg/A·year, indicating that its high efficiency is strongly linked to the as-cast microstructure.

B. Correlation with Microstructure and Electrochemical Data

The excellent performance of the as-cast 6 wt.% Si alloy is attributed to its fine Chinese-script Mg_2Si morphology, which promotes uniform dissolution [45]. T6 treatment disrupts this morphology, increasing Icorr from 3.62 to 4.64 μA/cm², consistent with the higher consumption rate. Visual examination supports these trends as shown in Figure 6-13, showing localized attack in high-consumption alloys and more uniform dissolution in efficient compositions.

Figure 6-13 Surface morphology of Al-6.5Mg-xSi sacrificial anode specimens (x = 1.5, 3, 6) after Anode performance measurement in both as-cast and T6 heat treated conditions.

Figure 6-13 validates the electrochemical results. As-cast alloys show non-uniform corrosion with localized pitting and crevice formation, consistent with higher consumption rates, with Al-6.5Mg-3Si exhibiting the maximum value of 5.0 kg/A·year. In contrast, T6-treated alloys display more uniform dissolution due to Mg_2Si redistribution, supported by shifts in Ecorr and Icorr (Table 6). This behavior is most pronounced in the Al-6.5Mg-6Si alloy, which achieved the highest anode capacity of 2781.5 A·h/kg.

6.2.6 Corrosion Mechanism in Al-Mg-SI alloy

Figures 6-14 illustrate the corrosion mechanism of Al-Mg-Si alloys in chloride media, where corrosion initiates at Mg_2Si particles due to chloride-induced oxide breakdown and propagates into the Al matrix, as confirmed by EDS analysis of Mg, Si-rich corrosion products. Corrosion susceptibility is governed by Mg_2Si morphology: fine, uniformly distributed particles (low Si) delay pit initiation and promote uniform attack, while coarse or continuous Mg_2Si networks (high Si) accelerate localized pitting and propagation [16,27]. The process evolves from initial Mg leaching at the Mg_2Si–Al interface to anodic dissolution of the surrounding Al matrix, with Si-enriched Mg_2Si transforming from anodic to cathodic sites over time, sustaining localized corrosion through occluded cell formation and chloride entrapment [49,50].

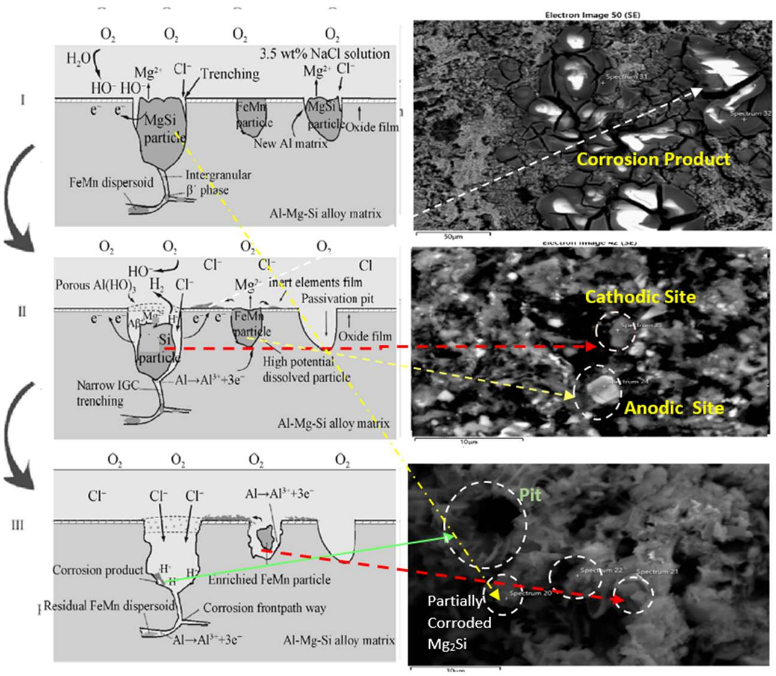

Figure 6-14. Schematic illustration of the corrosion mechanism in Al–Mg–Si alloys exposed to chloride solution. The yellow line marks initial anodic sites that later become cathodic regions (red line). Representative SEM images support the proposed mechanism.

7. ACHIEVEMENTS WITH RESPECT TO OBJECTIVES

1. Successfully developed Aluminum-Magnesium alloys with varying Silicon contents (1.5%, 3%, 4.5%, and 6%).

   Achieved a stable and fine Mg_2Si phase in the 6% Si alloy, ensuring uniform microstructure. Demonstrated controlled alloying and casting techniques that minimized defects and ensured reproducibility of the developed alloys.

2. Studied the effects of T6 heat treatment on the morphology of Mg_2Si phases.

   Observed that heat treatment leads to a transformation from fine, scattered Mg_2Si to coarser structures. Identified that while heat treatment modifies microstructure, it is detrimental for high Si (6%) alloy, as it accelerates self-corrosion and reduces the consumption efficiency of the anode.

3. Found that the 6% Silicon content acts as a natural stabilizer in the as-cast state.

   Achieved maximum driving potential and highest anode capacity without requiring additional heat treatment. Demonstrated the synergistic effect of alloying, where optimal Si content eliminates the need for secondary thermal processing while enhancing electrochemical performance.

8. CONCLUSIONS

The experimental results highlight the notable impact of silicon additions on the microstructure, hardness, and corrosion characteristics of Al–6.5%Mg alloys. Based on these findings, the following conclusions can be made:

1. Increasing Si content promoted the formation of Mg_2Si intermetallic phases, with morphology evolving from fine flakes to a well-developed Chinese-script eutectic at 6 wt.% Si in the as-cast condition. XRD and EDS confirmed the presence of α-Al, Mg_2Si, and Al_3Mg_2 phases.
2. Hardness increased with Si content and heat treatment due to precipitation strengthening, reaching a maximum of 107 HV for the Al-6.5Mg-6Si alloy after ageing.
3. Corrosion and electrochemical studies revealed that Mg_2Si morphology strongly influences corrosion behavior; coarse or continuous networks increased localized corrosion, while fine distributions promoted uniform dissolution. T6 heat treatment shifted corrosion potentials to more active values but increased dissolution rates.
4. Sacrificial anode testing demonstrated that the as-cast Al-6.5Mg-6Si alloy exhibits the best anodic performance, achieving the highest anode capacity (2781.5 Ah/kg) and lowest consumption rate (3.15 kg/A·year). Heat treatment significantly reduced anodic efficiency. Therefore, the as cast 6 wt.% Si alloy is optimal for sacrificial anode applications, whereas the heat-treated condition is better suited for strength-critical uses.

9. LIST OF PUBLICATIONS ARISING FROM THE RESEARCH

Sr No.	Name of Author	Title of Paper	Journal Name/Conference Proceeding Name	Volume (Edition), Page No. and Year	Publisher	Status	Other Details
1	Tushal K. Kyada, Indravadan B. Dave, and Sonam M. Patel	An Extensive Overview of Al-Mg-Si Alloy's Electrochemical Behavior	International Journal of Metallurgy and Alloys	Volume: 09, Issue-2, 2023	JournalsPub (**other**)	Published	ISSN no; 2456-5113 DOI: https://doi.org/10.37628/ijma.v9i2.1078

2	Tushal K. Kyada, Indravadan B. Dave, and Sonam M. Patel	Microstructure and Corrosion Behavior of Al, Al-Mg, and Al-Mg-Si Alloy as a Sacrificial Anode	Journal of the Maharaja Sayajirao University of Baroda: Science & Technology	Volume: 58, Page No.44-48 Year:2024	The Maharaja Sayajirao University of Baroda Vadodara, Gujarat, India (**UGC care**)	Published	ISSN no 0025-0422
3	Tushal K. Kyada, Indravadan B. Dave, Sonam M. Patel, Kunal Trivedi, Vandana J. Rao	Evaluating the Influence of Silicon on Phase Formation, Hardness and Corrosion in Al–6.5% Mg Alloy	Canadian Metallurgical Quarterly	-	Taylor & Fancis **(Scopus)**	Under Review	-
4	Tushal K. Kyada, Indravadan B. Dave, Sonam M. Patel	Synergistic Effect of Silicon Addition and Heat Treatment on Microstructure and Electrochemical Performance of Al–6.5Mg Alloy	Metallography, Microstructure, and Analysis.	-	Springer Nature (Scopus)	Under Review	

10. REFERENCES

1. Shreir LL, JRA, & BGT. Corrosion: Metal/Environment Reactions. 3rd ed. L.L. Shreir, R.A. Jarman, G.T. Burstein, editors. Elsevier; 2013.

2. Shuaib-Babata YL, Omokheni EI, Ambali IO, Busari YO, Abdulqadir LB, Ejiko SO, et al. Shuaib-Babata et al The effect of Magnesium addition on the performance of Aluminium-Zinc-Copper alloy as a sacrificial anode in seawater. J Mater Environ Sci. 2020;2020: 963–976.

3. Tsai T-M. Protection of Steel Using Aluminum Sacrificial Anodes in Artificial Seawater. J Mar Sci Technol. 1996;4. doi:10.51400/2709-6998.2545

4. GALVANIC (SACRIFICIAL) ANODE MATERIAL SELECTION AND DESIGN CONSIDERATIONS AND EXAMPLE CALCULATIONS (NON-MANDATORY). 2017.

5. https://themarineking.com/blogs/news/comparing-zinc-aluminum-and-magnesium-anodes.

6. Allen J B, Larry RF. Electrochemical Methods: Fundamentals and Applications. 2nd Edition. WILEY; 2000.

7. Marcel P. Atlas of electrochemical equilibria in aqueous solutions. 2nd ed. National Association of Corrosion Engineers; 1974.

8. Dehchar C, Charif D, Abdellatif L, Bouacida Walid Y. Electrochemical behavior of pure aluminum and aluminum alloy sacrificial anodes in seawater solution. 2018.

9. Prasad NK, Pathak AS, Kundu S, Panchal P, Mondal K. On the novel approach of sacrificial cathodic protection of mild steel in simulated concrete pore solution and concrete mortar by high phosphorus pig iron anodes. Journal of Materials Research and Technology. 2021;14: 582–608. doi:10.1016/J.JMRT.2021.06.070

10. Davis JR, Pdf JRD. ASM SPECIALTY HANDBOOK: ALUMINUM AND ALUMINUM ALLOYS DOWNLOAD EBOOK : ASM SPECIALTY HANDBOOK: ALUMINUM AND ALUMINUM ALLOYS.

11. Muazu A, Yaro. Effects of Zinc Addition on the Performance of Aluminium as Sacrificial Anode in Seawater. Journal of Minerals & Materials Characterization & Engineering. 2011.

12. Avner SH, Guatemala B, Lisbon H, Madrid L, New M, Panama D, et al. INTRODUCTION TO PHYSICAL METALLURGY Second Edition.

13. Aluminum and Aluminum Alloys Introduction and Overview. 2001. doi:10.1361/autb2001p351

14. Wen J, He J, Lu X. Influence of silicon on the corrosion behaviour of Al–Zn–In–Mg–Ti sacrificial anode. Corros Sci. 2011;53: 3861–3865. doi:10.1016/J.CORSCI.2011.07.039

15. Aceres CHC, Rovera DM. Solid solution strengthening in concentrated Mg±Al alloys. Available: www.elsevier.com/locate/lightmetals

16. Zheng Y, Luo B, Bai Z, Wang J, Yin Y. Study of the precipitation hardening behaviour and intergranular corrosion of Al-Mg-Si alloys with differing Si contents. Metals (Basel). 2017;7. doi:10.3390/met7100387

17. B6hni H, Uhlig HH. Environmental Factors Affecting the Critical Pitting Potential of Aluminum.

18. “V.A.Mistry” “Dr.M.S.Dani” “Dr.I.B.Dave.” A Review on Effect of Alloying Element on Aluminium Anode. International Conference on Recent Progress in Material Science and Mechanical Engineering. 2022;14th.

19. Umoru LE, Ige OO. Effects of Tin on Aluminum-Zinc-Magnesium Alloy as Sacrificial Anode in Seawater. Journal of Minerals & Materials Characterization & Engineering. 2007.

20. He JG, Wen JB, Li XD, Wang GW, Xu CH. Influence of Ga and Bi on electrochemical performance of Al-Zn-Sn sacrificial anodes. Transactions of Nonferrous Metals Society of China. 2011;21: 1580–1586. doi:10.1016/S1003-6326(11)60900-X

21. Polmear I, StJohn D, Nie J-F, Qian M. Light alloys: metallurgy of the light metals. Butterworth-Heinemann; 2017.

22. Gao G, Li Y, Wang Z, Di H, Li J, Xu G. Effects of the quenching rate on the microstructure, mechanical properties and paint bake-hardening response of Al-Mg-Si automotive sheets. Materials. 2019;12. doi:10.3390/ma12213587

23. Marioara CD, Andersen SJ, Jansen J, Zandbergen HW. The influence of temperature and storage time at RT on nucleation of the β″ phase in a 6082 Al–Mg–Si alloy. Acta Mater. 2003;51: 789–796. doi:10.1016/S1359-6454(02)00470-6

24. Deschamps A, Brechet Y. Influence of predeformation and agEing of an Al–Zn–Mg alloy—II. Modeling of precipitation kinetics and yield stress. Acta Mater. 1998;47: 293–305. doi:10.1016/S1359-6454(98)00296-1

25. ’William S ’Javad, H. Foundations of Materials Science and Engineering. 7th edition. 2023.

26. El Garchani FE, Lgaz H, Kaya S, Lee HS, Ibrahim SM, Chafiq M, et al. Effects of heat treatment on the corrosion behavior and mechanical properties of aluminum alloy 2024. Journal of Materials Research and Technology. 2023;25: 1355–1363. doi:10.1016/J.JMRT.2023.05.278

27. Zeng FL, Wei ZL, Li JF, Li CX, Tan X, Zhang Z, et al. Corrosion mechanism associated with Mg 2Si and Si particles in Al-Mg-Si alloys. Transactions of Nonferrous Metals Society of China (English Edition). 2011;21: 2559–2567. doi:10.1016/S1003-6326(11)61092-3

28. Tebib M, Samuel AM, Ajersch F, Chen XG. Effect of P and Sr additions on the microstructure of hypereutectic Al-15Si-14Mg-4Cu alloy. Mater Charact. 2014;89: 112–123. doi:10.1016/j.matchar.2014.01.005

29. Li Z, Li C, Liu Y, Yu L, Guo Q, Li H. Effect of heat treatment on microstructure and mechanical property of Al–10%Mg2Si alloy. J Alloys Compd. 2016;663: 16–19. doi:10.1016/J.JALLCOM.2015.12.128

30. Sun Y, Hu M, Li M, Li C, Zhu X, Xia X, et al. The effect of solution temperature on the precipitates evolution and aging hardening response of Al-15%Mg2Si(-1%Cu) alloys. Journal of Materials Research and Technology. 2022;17: 1330–1337. doi:10.1016/J.JMRT.2022.01.094

31. Jarco A, Pezda J. Effect of heat treatment process and optimization of its parameters on mechanical properties and microstructure of the alsi11(Fe) alloy. Materials. 2021;14. doi:10.3390/ma14092391

32. Alshibli MJ, Gebril MA, Shuaeib FM. Aluminum 6063 Alloy Production Optimization-Part I: The Casting Process. International Journal of Current Science (IJCSPUB) www.ijcspub.org. 2024.

33. Maisonnette D, Suery M, Nelias D, Chaudet P, Epicier T. Effects of heat treatments on the microstructure and mechanical properties of a 6061 aluminium alloy. Materials Science and Engineering: A. 2011;528: 2718–2724.doi:10.1016/J.MSEA.2010.12.011

34. Feuerbacher M, Thomas C, Makongo JPA, Hoffmann S, Carrillo-Cabrera W, Cardoso R, et al. The Samson phase, β-Mg2Al3, revisited. Zeitschrift fur Kristallographie. 2007. pp. 259–288. doi:10.1524/zkri.2007.222.6.259

35. Zheng Y, Luo B, Bai Z, Wang J, Yin Y. Study of the precipitation hardening behaviour and intergranular corrosion of Al-Mg-Si alloys with differing Si contents. Metals (Basel). 2017;7. doi:10.3390/met7100387

36. Seth PP, Parkash O, Kumar D. Structure and mechanical behavior ofin situdeveloped Mg2Si phase in magnesium and aluminum alloys - a review. RSC Advances. Royal Society of Chemistry; 2020. pp. 37327–37345. doi:10.1039/d0ra02744h

37. Edwards GA, Stiller K, Dunlop GL, Couper MJ. THE PRECIPITATION SEQUENCE IN Al±Mg±Si ALLOYS.

38. Gao YH, Zhang XX, Lv Y, Xu P, Zhao YF, Zhang YP, et al. Distinctive localized corrosion behavior of β-Mg2Si and α-Al(Fe,Mn)Si phases in a 6082 alloy. Journal of Materials Research and Technology. 2024;29: 1675–1682. doi:10.1016/J.JMRT.2024.01.217

39. Kairy SK, Birbilis N. Clarifying the Role of Mg2Si and Si in Localized Corrosion of Aluminum Alloys by Quasi In Situ Transmission Electron Microscopy. Corrosion. 2020;76: 464–475. doi:10.5006/3457

40. Wu Y, Shen Y, Wang Q, Liu Y, Shi D, Liu Y, et al. Effect of Si Content on Microstructures and Electrochemical Properties of Al-xSi-3.5Fe Coating Alloy. Materials. 2023;16. doi:10.3390/ma16237407

41. Jang K-S, Jang T, Jo H, Shin D, Lee S, Kim S-D, et al. Effect of Heat Treatment on Corrosion Resistance of A356 Casting Alloy. Materials. 2025;18: 1056. doi:10.3390/ma18051056

42. Wu L, Oliveira JP, Yang J, Xiao M, Zheng M, Xu W, et al. Effect of Al-Si Coating on the Interfacial Microstructure and Corrosion Resistance of Dissimilar Laser Al Alloy/22MnB5 Steel Joints. Metals (Basel). 2024;14. doi:10.3390/met14030328

43. Ikeuba AI, Njoku CN, Ekerenam OO, Njoku DI, Udoh II, Daniel EF, et al. A review of the electrochemical and galvanic corrosion behavior of important intermetallic compounds in the context of aluminum alloys. RSC Advances. Royal Society of Chemistry; 2024. pp. 31921–31953. doi:10.1039/d4ra06070a

44. “LI Chaoxing” “LI Jinfeng”, “BIRBILIS Nick”, “JIA Zhiqiang”, “ZHENG Ziqiao.” SYNERGETIC EFFECT OF Mg2Si AND Si PARTICLES ON INTERGRANULAR CORROSION OF Al-Mg-Si ALLOYS THROUGH MULTI-ELECTRODE COUPLING SYSTEM. J Chin Soc Corr Pro. 2010;30: 107–113.

45. Li C, Sun J, Li Z, Gao Z, Liu Y, Yu L, et al. Microstructure and corrosion behavior of Al–10%Mg2Si cast alloy after heat treatment. Mater Charact. 2016;122: 142–147. doi:10.1016/j.matchar.2016.10.027

46. Revilla RI, Verkens D, Rubben T, De Graeve I. Corrosion and corrosion protection of additively manufactured aluminium alloys—a critical review. Materials. MDPI AG; 2020. pp. 1–25. doi:10.3390/ma13214804

47. Sekhar AP, Mandal AB, Das D. Mechanical properties and corrosion behavior of artificially aged Al-Mg-Si alloy. Journal of Materials Research and Technology. 2020;9: 1005–1024. doi:10.1016/j.jmrt.2019.11.040

48. Wei P, Chen Z, Zhang S, Fang X, Lu B, Zhang L, et al. Effect of T6 heat treatment on the surface tribological and corrosion properties of AlSi10Mg samples produced by selective laser melting. Mater Charact. 2021;171: 110769. doi:10.1016/J.MATCHAR.2020.110769

49. Vacchi GS, Silva R, Plaine AH, Suhuddin UFH, Alcântara NG, Sordi VL, et al. Refill friction stir spot welded AA5754-H22/Ti-6Al-4V joints: Microstructural characterization and electrochemical corrosion behavior of aluminum surfaces. Mater Today Commun. 2020;22: 100759. doi:10.1016/J.MTCOMM.2019.100759

50. Vacchi GS, Plaine AH, Silva R, Sordi VL, Suhuddin UFH, Alcântara NG, et al. Effect of friction spot welding (FSpW) on the surface corrosion behavior of overlapping AA6181-T4/Ti-6Al-4V joints. Mater Des. 2017;131: 127–134. doi:10.1016/J.MATDES.2017.06.005